Vibronic coupling in the superoxide anion: The vibrational dependence of the photoelectron angular distribution

Matthew Van Duzor,[1] Foster Mbaiwa,[1] Jie Wei,[1] Tulsi Singh,[1] Richard Mabbs,[1,a)] Andrei Sanov,[2] Steven J. Cavanagh,[3] Stephen T. Gibson,[3] Brenton R. Lewis,[3] and Jason R. Gascooke[4]

[1]*Department of Chemistry, Washington University, One Brookings Dr., Campus Box 1134 Saint Louis, Missouri 63130, USA*
[2]*Department of Chemistry and Biochemistry, University of Arizona, Tucson, Arizona 85721-0041, USA*
[3]*Research School of Physics and Engineering, The Australian National University, Canberra, Australian Capital Territory 0200, Australia*
[4]*School of Chemical and Physical Sciences, Flinders University, G.P.O. Box 2100, Adelaide, South Australia 5001, Australia*

(Received 20 April 2010; accepted 3 September 2010; published online 3 November 2010)

We present a comprehensive photoelectron imaging study of the $O_2(X\,^3\Sigma_g^-, v'=0-6) \leftarrow O_2^-(X\,^2\Pi_g, v''=0)$ and $O_2(a\,^1\Delta_g, v'=0-4) \leftarrow O_2^-(X\,^2\Pi_g, v''=0)$ photodetachment bands at wavelengths between 900 and 455 nm, examining the effect of vibronic coupling on the photoelectron angular distribution (PAD). This work extends the $v'=1-4$ data for detachment into the ground electronic state, presented in a recent communication [R. Mabbs, F. Mbaiwa, J. Wei, M. Van Duzor, S. T. Gibson, S. J. Cavanagh, and B. R. Lewis, Phys. Rev. A **82**, 011401(R) (2010)]. Measured vibronic intensities are compared to Franck–Condon predictions and used as supporting evidence of vibronic coupling. The results are analyzed within the context of the one-electron, zero core contribution (ZCC) model [R. M. Stehman and S. B. Woo, Phys. Rev. A **23**, 2866 (1981)]. For both bands, the photoelectron anisotropy parameter variation with electron kinetic energy, $\beta(E)$, displays the characteristics of photodetachment from a *d*-like orbital, consistent with the π_g^* $2p$ highest occupied molecular orbital of O_2^-. However, differences exist between the $\beta(E)$ trends for detachment into different vibrational levels of the $X\,^3\Sigma_g^-$ and $a\,^1\Delta_g$ electronic states of O_2. The ZCC model invokes vibrational channel specific "detachment orbitals" and attributes this behavior to coupling of the electronic and nuclear motion in the parent anion. The spatial extent of the model detachment orbital is dependent on the final state of O_2: the higher the neutral vibrational excitation, the larger the electron binding energy. Although vibronic coupling is ignored in most theoretical treatments of PADs in the direct photodetachment of molecular anions, the present findings clearly show that it can be important. These results represent a benchmark data set for a relatively simple system, upon which to base rigorous tests of more sophisticated models. © *2010 American Institute of Physics*. [doi:10.1063/1.3493349]

I. INTRODUCTION

The coupling between electronic and vibrational degrees of freedom often affects the spectroscopic and structural properties of molecules. However, experimental evidence of vibrational influence on the photoelectron angular distributions (PADs) in negative-ion photodetachment has so far been sparse, and little attention has been paid to such effects in theoretical treatments of direct detachment processes. In a recent communication,[1] we reported a strong dependence of the PADs in $O_2^-(X\,^2\Pi_g, v''=0)$ photodetachment on the final vibrational state of the neutral, $O_2(X\,^3\Sigma_g^-, v'=1-4)$. These results provided experimental evidence of vibronic coupling in the anion ground electronic state, supplying essential data for the evaluation and refinement of existing theoretical models.

In the present work, we extend the above measurements to include the additional $v'=0$, 5, and 6 transitions of the $O_2(X\,^3\Sigma_g^-) \leftarrow O_2^-(X\,^2\Pi_g)$ band and the $v'=0-4$ transitions of the excited-state $O_2(a\,^1\Delta_g) \leftarrow O_2^-(X\,^2\Pi_g)$ band. We present a new, detailed discussion of these results in the context of the zero core contribution (ZCC) model,[2] complementing our previous analysis.[1] In addition, the observed trend in vibronic transition intensities in the $O_2(X\,^3\Sigma_g^-) \leftarrow O_2^-(X\,^2\Pi_g)$ band is evaluated.

The dominant long range interaction in anion photodetachment is associated with the centrifugal term in the effective potential.[3] The nature of the long range potential significantly affects the energy dependence of the total[4] and differential detachment cross sections.[5] In fact, the application of orbital angular momentum conservation and consideration of the influence of the centrifugal barrier in principle allows the characterization of the parent orbital from the photoelectron angular distribution.[5–7] Within the one-electron and electric-dipole approximations, the PAD of an atomic anion detachment can be thought of as a signature of the parent orbital.[8]

a)Electronic mail: mabbs@wustl.edu.

The relationship between the parent orbital and the PAD is in principle more complex for molecular anions.[9,10] Orbital angular momentum (ℓ) is no longer a good quantum number, and the vibrational excitation often accompanies the change in electronic state. The application of symmetry arguments can still act as a guide to the nature of the parent molecular orbital.[11–18] More subtle effects, such as the influence of the final, neutral molecular state are often difficult to extract. There are, however, a few small molecular anions that might allow detailed experimental studies into these effects.

In the case of superoxide, O_2^-, the highest occupied molecular orbital (π_g) has a strong similarity to an atomic d orbital. There is only one vibrational degree of freedom, and photoelectron-spectroscopic techniques are capable of resolving the vibrational structure in the low electron kinetic energy region of the spectrum. A comparison of O_2^- photodetachment results with atomic anion model predictions yields considerable insight into the effect of vibrational excitation on the photodetachment properties, in particular the PAD.[1]

Several detachment studies of this species have probed the photon energy dependence of the total detachment cross section[19–26] or reported the photoelectron spectrum of O_2^-.[1,27–38] Until very recently, much less data were reported regarding the PAD.[1,28,35] Among other anions, the prominent dependence of photoelectron anisotropy on the final vibrational state of the neutral was reported in the photodetachment of NO^-.[39] In the case of neutral diatomic molecules, dramatic changes in the PAD have been observed between different vibronic photoionization bands of N_2, CO, and O_2.[40–42] Such effects are associated with strong coupling of the electronic and vibrational motion and usually a breakdown of the Born–Oppenheimer approximation as a consequence of excitation of intermediate, autoionizing Rydberg states or shape resonances.[42]

It is well known that the PAD is dependent on electron kinetic energy (E).[43] To separate the effect of vibrational excitation from the E dependence, one must, ideally, compare transitions that terminate in different vibrational states but correspond to the same E. This approach requires experiments at multiple, carefully selected photoexcitation wavelengths. Studies of this type are rarely performed, particularly for molecular anions. Despite the work reported in Ref. 44 for photoionization, the prevalent view seems to have been that in the absence of vibrationally resolved data in direct photodetachment processes, vibrational effects on the PAD can be ignored.

A comparison of near-threshold PADs of O_2^- recorded at different excitation wavelengths shows that this view is shortsighted.[1,35] Figure 1 compares anisotropy parameter (β) data for the $O_2(X\ ^3\Sigma_g^-) \leftarrow O_2^-(X\ ^2\Pi_g)$ vibronic band at detachment wavelengths 780 nm (open circles), 396 nm (closed circles),[35] and 488 nm (open squares).[28] β characterizes the PAD, and a change is clearly seen in the 780 nm data. However, if the PAD were dependent only on the parent (π_g) orbital and E, one would expect β to be constant within the $X \leftarrow X$ band for a given E, regardless of the detachment wavelength and, therefore, the final vibrational state of the neutral. Nonetheless, distinctly different β values are observed for comparable E but different final vibrational states.

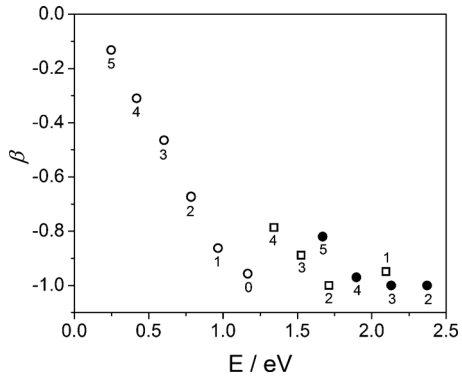

FIG. 1. Comparison of anisotropy parameters associated with detachment from the π_g orbital of O_2^- at 780 nm (open circles), 396 nm (filled circles) from Ref. 35, and 488 nm (open squares) from Ref. 28 via the $O_2(X\ ^3\Sigma_g^-, v') \leftarrow O_2^-(X\ ^2\Pi_g, v''=0)$ transition. Numeric labels represent v'.

The more recent study of the E evolution of the angular distributions associated with photodetachment via the $O_2(X\ ^3\Sigma_g^-) \leftarrow O_2^-(X\ ^2\Pi_g)$ band has clearly shown that the level of vibrational excitation of the neutral molecule influences the angular distributions associated with direct detachment from the superoxide anion.[1]

While several theoretical treatments have been developed to treat photoelectron angular distributions from diatomic molecules, the effect of accompanying vibrational excitation is almost completely ignored (with the notable exception of Ref. 44), presumably in part due to a lack of experimental data. Anion detachment studies have tended to focus either on the nature of the parent orbital itself or on the effects of momentum transfer in rare cases of rotationally resolved detachment spectra. Momentum transfer formalisms[7,45–50] have been used to explain the differential cross section (angular distribution) for photoelectrons produced in rotationally resolved[51] and nonrotationally resolved[52,53] H_2 spectra. The effect of spin polarization of the photoelectrons has also been taken into account in rotationally resolved molecular photoelectron spectra.[54] More recent treatments of O_2^- photodetachment include single and multichannel scattering calculations using Schwinger variational methods[55] and calculation of the radial matrix elements for the central-potential model of Cooper and Zare using Dyson orbitals computed via coupled-cluster equation of motion methods.[56] Only in the application of the ZCC model[57] to diatomic anion photodetachment has the effect of vibrational excitation on the angular distribution been quantified.[2] The systematic test of the predicted $\beta(E)$ trends for each vibronic transition associated with the $O_2(X\ ^3\Sigma_g^-) \leftarrow O_2^-(X\ ^2\Pi_g)$ band, begun in Ref. 1 and extended and discussed in greater depth here, is hoped to stimulate further theoretical interest in this phenomenon.

II. EXPERIMENTAL METHODS

O_2^- photoelectron images were recorded over a range of detachment wavelengths between 900 and 455 nm in small intervals. The precise determination of β requires care. The extracted value is sensitive to a variety of possible experimental artifacts.[58,59] To minimize the influence of such effects and to verify the repeatability of our observations, in-

dependent measurements were recently reported from two different laboratories in St. Louis (USA) and Canberra (Australia).[1]

The results presented here were recorded on the Canberra instrument and extend the data set to the $O_2(X\,^3\Sigma_g^-, v') \leftarrow O_2^-(X\,^2\Pi_g, v''=0)$, $v'=0,5,6$ transitions, and $O_2(a\,^1\Delta_g, v') \leftarrow O_2^-(X\,^2\Pi_g, v''=0)$, $v'=0-4$ band. The instrumentation has been described previously,[58] and only brief details will be provided. Essentially, the apparatus produces a collimated beam of mass-selected negative ions, which can then be interrogated by a laser beam, subsequently producing photoelectrons. The photodetached electrons are imaged onto a multichannel-plate (MCP) phosphor detector using a modified velocity-map imaging lens.

Molecular oxygen anions are produced by passing pure oxygen gas through a pulsed nozzle (General Valve Series 9) at a stagnation pressure of 2.7 atm and then supersonically expanding it through a pulsed discharge.[58] All negative ions are extracted, accelerated to 500 eV, focused into an ion-gating, bunching, and potential rereferencing unit,[60] and allowed to propagate along a ground-referenced 2 m time-of-flight (TOF) tube. The ion-beam and imaging lens axes are arranged coaxially. A fast potential switch rereferences the ion packet to the imaging assembly repeller-plate potential. A potential barrier is placed between the second potential switch and the repeller plate of the imaging lens. This acts, when switched together with the potential switch, as a mass discriminator, allowing only the mass of interest to enter the imaging lens.

The mass-selected ion packet intersects the detachment laser beam, generated by a Continuum Sunlite EX optical parametric oscillator, which is pumped by a Powerlite 9010 Nd:yttrium aluminum garnet laser, operated at its third harmonic, 355 nm. The laser operates between 1 and 3 mJ per pulse and at 10 Hz. To ensure a very high degree of polarization parallel to the MCP detector face, the laser beam was passed through a 1/2-waveplate and a high-quality broad bandwidth Glan-Laser polarizer. A Galilean telescope arrangement is used to produce a parallel beam of 2 mm diameter, reduced from the laser diameter of 8 mm. The wavelength of the laser is measured using a high-quality wavemeter (High Finesse WS7 UV).

The high resolution velocity-map imaging lens is a substantially modified version of Eppink and Parker's arrangement.[61] It was designed to accommodate fast ion-beam energies of 10^2-10^3 eV and an increased interaction region volume size (at least 2 mm^3), achieving electron kinetic energy resolutions of $\Delta E/E \approx 0.3\%$ or better. Photoelectrons are imaged onto a position sensitive detector consisting of a pair of high dynamic range, imaging quality 10 μm-pore MCPs, a P47 phosphor screen, and a 2048 $\times$2048-pixel monochrome charge coupled device camera (PCO2000). The imaging detector is situated at the end of the TOF tube, 800 mm from the interaction region, and is shielded from magnetic fields through a combination of μ-metal and three orthogonal Helmholtz coils. The MCP gain is gated using a purpose-built fast high-voltage pulser to coincide with the arrival of the photoelectrons. This ensures that unwanted events from ions or neutral species are not detected. Each camera frame is transferred to a PC at the 10 Hz repetition rate and is processed in real time to identify events, centroiding to subpixel accuracy, with the x-, y-coordinates written to a file, for subsequent analysis.

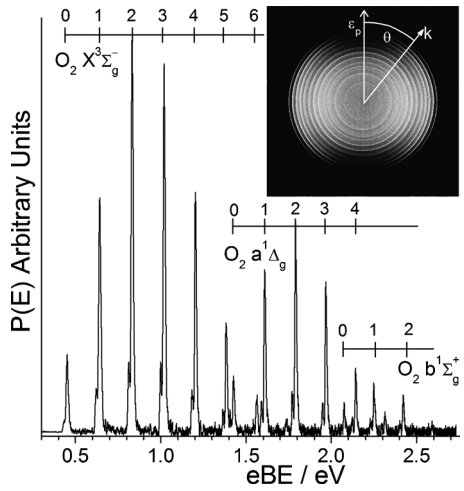

FIG. 2. 454.57 nm raw image of O_2^- detachment. The corresponding photoelectron spectrum is shown below as a function of electron binding energy.

III. RESULTS AND ANALYSIS

The photoelectron images obtained in this study were recorded at detachment wavelengths of 454.57, 489.56, 531.79, 629.89, 679.72, 750.90, 800.87, 850.88, and 901.22 nm. A typical image is shown in Fig. 2 (454.57 nm). Lighter colored areas of the image indicate higher photoelectron intensity.

The use of linearly polarized photons confers cylindrical symmetry upon the laboratory frame (LF) photoelectron momentum distribution. The raw image in Fig. 2 is an Abel transform of the three-dimensional LF distribution, a two-dimensional projection onto the plane of the detector. The LF distribution can be mathematically reconstructed by applying the inverse transform. The inverse transformation is performed using the Hansen and Law algorithm,[62] and photoelectron spectra are then extracted.

A. Photoelectron spectra

The momentum domain spectrum is obtained from the reconstructed image by integration over $\theta=0-2\pi$ at all radii, where θ is defined as the angle between the laser polarization axis ($\vec{\boldsymbol{\varepsilon}}_\mathbf{p}$, vertical in the plane of the image) and the momentum vector of the electron. The conversion to the energy domain is effected using the appropriate Jacobian transformation.

The spectrum in Fig. 2 is displayed as a function of electron binding energy, $eBE=h\nu-E$. A detachment from the superoxide anion (at the photon energies employed here) removes an electron from the antibonding π_g orbital. Consequently, the equilibrium bond length is shorter in the neutral $O_2(X\,^3\Sigma_g^-: R_e' = 1.2075$ Å) compared to the anion ($X\,^2\Pi_g: R_e'' = 1.348$ Å) (Ref. 27) and vibrational excitation accompanies the detachment process, resulting in significant population of up to six vibrational quanta, as seen in the

vibrational progression in the $O_2(X\ ^3\Sigma_g^-) \leftarrow O_2^-(X\ ^2\Pi_g, v''=0)$ band. The vibronic transitions are clearly seen in the image as a series of concentric rings, with the larger rings corresponding to lower levels of internal excitation in the neutral O_2. These features are clear in the spectrum, which also resolves transitions from the two spin-orbit states ($^2\Pi_{g,\Omega=3/2,1/2}$) of the anion.

The spectral intensities are normalized relative to the $O_2(X\ ^3\Sigma_g^-, v'=2) \leftarrow O_2^-(X\ ^2\Pi_g, v''=0)$ transition. Three vibronic bands are visible in the portion of the spectrum shown in Fig. 2, which correspond to detachment via the ground ($X\ ^3\Sigma_g^-$) and first two excited ($a\ ^1\Delta_g$, b $^1\Sigma_g^+$) electronic states of O_2.

B. The photoelectron angular distributions

It is clear in the image in Fig. 2 that the photoelectron intensity is not necessarily constant about a ring of given radius. This is particularly obvious in the outer rings in the image in Fig. 2, where the intensity is greatest at $\theta=\pi/2$. The intensity distribution, $I(E,\theta)$ is a measure of the differential cross section for detachment and is described by

$$I(E,\theta) = \frac{\sigma(E)}{4\pi}[1+\beta(E)P_2(\cos\ \theta)], \tag{1}$$

where σ is the integrated cross section and P_2 is the second Legendre polynomial. The anisotropy parameter β is determined by the details of the detachment process and characterizes the angular distribution. Any effects of the detachment process on the angular distribution can therefore be conveniently discussed in terms of changes in the anisotropy parameter.

In this work, we focus on the PADs accompanying the $O_2(X\ ^3\Sigma_g^-) \leftarrow O_2^-(X\ ^2\Pi_g)$ vibronic transitions of O_2^- detachment. However, Fig. 4 shows that the $O_2(a\ ^1\Delta_g) \leftarrow O_2^-(X\ ^2\Pi_g)$ vibronic transitions display a similar behavior. The apparent changes in $\beta(E)$ trends have significant implications for theoretical treatments of the detachment process. The anisotropy parameter is extracted by plotting $I(E,\theta)$ against $P_2(\cos\ \theta)$ at a given E. We note that the β values reported in this work differ slightly from those previously reported.[28,35] This is not too surprising, considering that β values are very sensitive to image distortion (imparted by external fields or imperfect focusing) and detector saturation. In the present work, extreme care has been applied to minimize such adverse effects. The images are circularized to eliminate distortion effects.[58] Additionally, saturation effects are easily identified as deviations from linearity at the extremes of the angular range in a plot of $I(E,\theta)$ versus $P_2(\cos\ \theta)$, and we note that none of the images reported here display any evidence of saturation. Furthermore, the results have been verified independently in the different laboratories of the authors, with each set of measurements being in excellent agreement.[1]

For the remainder of this work, we focus on the relationship between β and E and in particular the effect that the level of vibrational excitation of the neutral residue seems to exert. In Fig. 3, we show the variation of β with E for the $O_2(X\ ^3\Sigma_g^-) \leftarrow O_2^-(X\ ^2\Pi_g)$ band. All data shown are for transitions originating in the $O_2^-(X\ ^2\Pi_{g,\Omega=3/2})v''=0$ spin-orbit state. The neutral O_2 vibrational levels accessed are (a) $v'=0$, (b) $v'=1$, (c) $v'=2$, (d) $v'=3$, (e) $v'=4$, (f) $v'=5$, and (g) $v'=6$. A change in β with E is not unexpected. More surprising, at least in the light of the expectation that the PAD depends on the parent π_g orbital only, is the difference in β seen in Fig. 3(h) for different vibronic transitions at comparable E. Figure 4 shows similar behavior in the $O_2(a\ ^1\Delta_g, v') \leftarrow O_2^-(X\ ^2\Pi_g, v''=0)$ band for $v'=0-4$.

There is an initial shift toward increasingly negative values until a minimum is reached (at least for the $v'=0$ and $v'=1$ series) before becoming less negative. However, the rate of change of β in each case is different. For E between 0 and 1.5 eV, lower v' correspond to more negative β. Clearly, accessing different terminal neutral states has a profound influence on the photoelectron angular distribution.

IV. DISCUSSION

The E dependence of β when $\ell>0$ has been previously demonstrated in atomic anion detachment experiments.[58,63–68] In these cases, the change in β can be explained through consideration of the dominant long range term in the potential, the centrifugal term. The free electron wave can be represented as a superposition of partial angular momentum waves for which we will use the symbol ℓ' ($=\ell\pm1$) to allow distinction from the parent orbital angular momentum quantum number ℓ. The centrifugal barrier increases with ℓ' and decreases with distance. In the asymptotic limit, the barrier is therefore zero, but in the near-field limit, the barrier leads to different contributions of the partial waves to the overall superposition. According to the Wigner law,[4] at the detachment threshold the cross section of each partial wave varies as $\sigma_{\ell'} \propto E^{(\ell'+1/2)}$. The angular distribution, and hence β, is the result of interference between these partial waves, and so changing the composition of the superposition changes the angular distribution. For atomic anions, this behavior is encapsulated in the equation

$$\beta(E) = \frac{\ell(\ell-1)+(\ell+1)(\ell+2)A^2\cdot E^2 - 6\ell(\ell+1)A\cdot E\cos\ \delta_{(\ell+1)-(\ell-1)}}{(2\ell+1)[\ell+(\ell+1)A^2\cdot E^2]}. \tag{2}$$

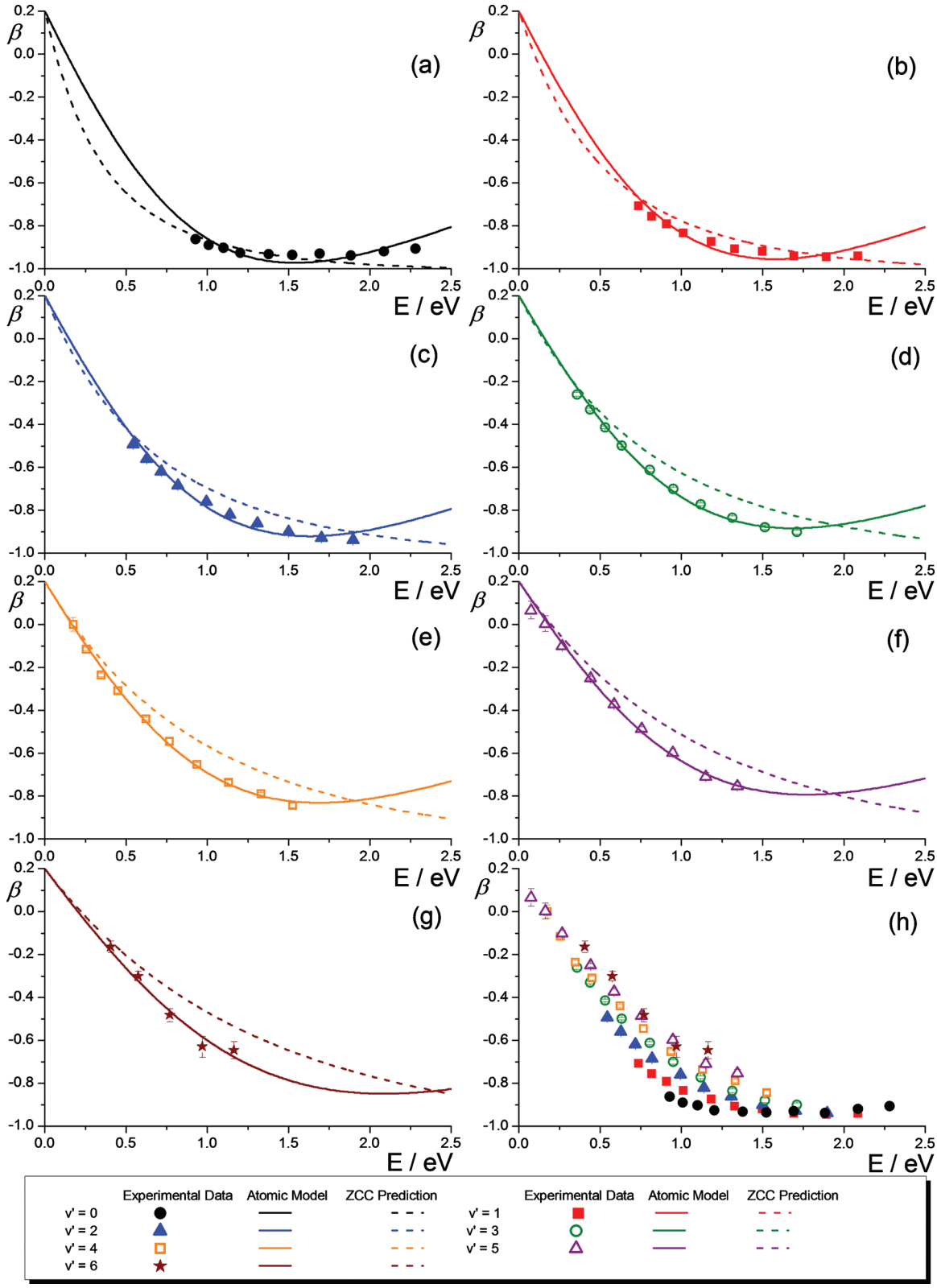

FIG. 3. Variation in β with E for $O_2(X\,^3\Sigma_g^-, v') \leftarrow O_2^-(X\,^2\Pi_g, v''=0)$ transitions. [(a)–(g)] $v'=0$–6, respectively. Experimental data are indicated by symbols, and, where absent, error bars are smaller than the symbols. Solid curves represent the fit of an atomic model to these data. Dashed curves represent the predictions of the ZCC model. (h) Direct comparison of $v'=0$–6.

This is a simplification of the result of an approach initially outlined by Bethe[5] for single-electron atoms, later generalized to multielectron atoms[6,7,43,69] and with the approximation that the relative partial ℓ' wave cross sections ($\sigma_{\ell\pm1}$) obey the Wigner threshold behavior within a few eV of threshold,[65] so that $\sigma_{\ell+1}/\sigma_{\ell-1}=A\cdot E$. The physical picture behind Eq. (2) is the interference of the two partial electron waves, which of course depends on the relative cross sections (carried through the $A\cdot E$ term) and their relative phase shift, $\delta_{(\ell+1)-(\ell-1)}$.[8]

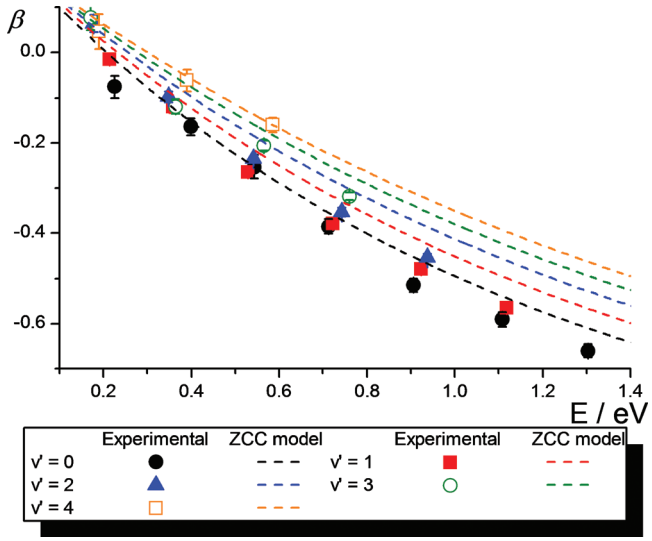

FIG. 4. Variation in β with E for $O_2(a\ ^1\Delta_g, v'=0-4) \leftarrow O_2^-(X\ ^2\Pi_g, v''=0)$ transitions. Experimental data are indicated by symbols, and, where absent, error bars are smaller than the symbols. Dashed curves represent the predictions of the ZCC model.

In the case of molecular anion detachment, the interpretation of the PAD is generally complicated by the loss of spherical symmetry of the potential. Although, as previously identified, ℓ is not generally a "good" molecular quantum number, the π_g highest occupied molecular orbital of O_2^- bears a strong intuitive resemblance to an atomic d orbital. It might therefore be expected that Eq. (2) can be used to describe the observed E dependence of β using $\ell=2$ and the appropriate empirically determined values of A and δ. Indeed, the experimental intercept ($E=0$ in Fig. 3) value is approximately +0.2, for which Eq. (2) implies that $\ell=2$.[44]

For brevity and clarity, in the following, we frame the discussion in terms of the $O_2(X\ ^3\Sigma_g^-) \leftarrow O_2^-(X\ ^2\Pi_g)$ band. However, this discussion is also applicable to the $O_2(a\ ^1\Delta_g) \leftarrow O_2^-(X\ ^2\Pi_g)$ detachment. The results of nonlinear least-squares fitting (via the Levenberg–Marquardt algorithm) of Eq. (2) to the $O_2(X\ ^3\Sigma_g^-) \leftarrow O_2^-(X\ ^2\Pi_g)$ band data are shown in Figs. 3(a)–3(g). Values of A, $\cos\delta_{(\ell+1)-(\ell-1)}$, and an indication of the quality of the fit through RR^2, the reduced coefficient of determination, are given in Table I. In general, the fits are very good, suggesting that the atomic picture of detachment (at least in terms of the electronic orbital) is a reasonable first approximation that reproduces the essential trends in the data.

A and $\cos\delta_{(\ell+1)-(\ell-1)}$ show a systematic decrease as the vibrational excitation of the neutral O_2 residue increases. However, while satisfactory agreement with the atomic model can be obtained for each vibronic transition, the required fitting coefficients offer no physical explanation for the observed vibrational dependence. In particular, the decrease in the value of A in the framework of the atomic model suggests a decrease in the "size" of the parent anion.[65] This indication needs to be reconciled with the fact that the spatial extent of the neutral (O_2) nuclear wave function increases with increasing v'.

The differential cross section (the cross section for photodetachment of an electron into a particular solid angle Ω) is related to the electronic transition matrix element, M^e by

$$\frac{d\sigma}{d\Omega} \propto F(v',v'')k\omega \int |M^e|^2 d\Omega_m. \tag{3}$$

The measured angular distribution arises through averaging over all orientations (Ω_m) of the parent molecular anion in the laboratory frame. $F(v',v'')$ is the well known Franck–Condon factor, which is orientation independent. k is the linear momentum of the photoelectron, and ω is the photon frequency.

Since the Franck–Condon factors are also E-independent, the energy dependence of the differential cross section (and hence photoelectron angular distribution) must be contained in the electronic transition matrix element. Within the one-electron approximation, M^e is equivalent to[2]

$$M^e = \int\int\int \phi_k^* \vec{\boldsymbol{\varepsilon}}_{\mathbf{p}} \cdot \vec{\mathbf{r}} \phi_{do}(\vec{\mathbf{r}};R_{OO}) r^2 \sin\theta d\phi d\theta dr. \tag{4}$$

The bound excess electron wave function (the detachment orbital) is represented by ϕ_{do}, and the free electron wave function is represented by ϕ_k.

A relatively simple quantitative assessment of the effect of vibrational excitation can be made by applying the zero core contribution model to evaluate Eq. (4).[57] A core region is defined, within which the detachment orbital is assumed to have negligible amplitude. The integration is carried out numerically (with a Gauss–Laguerre quadrature) over regions outside the core.[70] As in Ref. 2, we calculate the β parameter by representing the free electron as a plane wave, and the core region is determined using two overlapping spheres (radii of 0.96 Å) centered on the O atoms. To account for the vibrational effects, each vibronic channel of the detachment process is represented by its own initial (bound) wave function of the detached electron, termed the "detachment or-

TABLE I. Parameters associated with fitting Eq. (2) to the experimental data in Fig. 3. Uncertainties in the last significant figure are given in parentheses. RR^2 is the reduced coefficient of determination associated with the fit.

	v'						
	0	1	2	3	4	5	6
A (eV^{-1})	0.43(2)	0.42(1)	0.40(1)	0.389(7)	0.39(1)	0.36(2)	0.31(5)
$\cos\delta_{(\ell+1)-(\ell-1)}$	0.981(7)	0.969(7)	0.945(8)	0.919(7)	0.88(1)	0.86(2)	0.89(9)
RR^2	0.9919	0.9925	0.9943	0.9978	0.9973	0.9959	0.9894

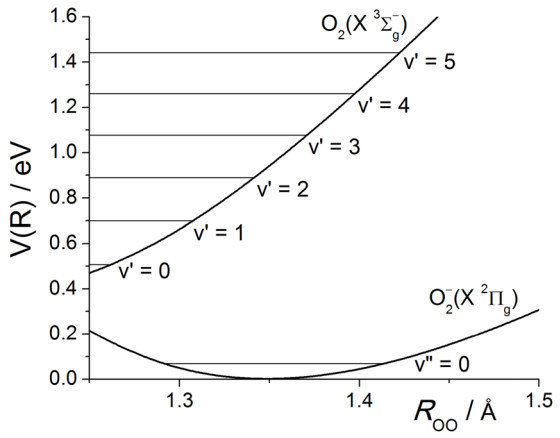

FIG. 5. Potentials and vibrational levels for the ground states of O_2^- and O_2.

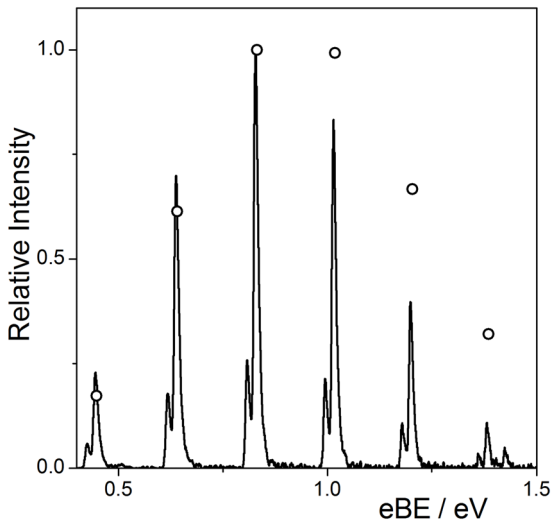

FIG. 6. Comparison of relative Franck–Condon factors (open circles) and 2.73 eV (454.57 nm) O_2^- spectrum.

bital." We approximate the detachment orbital using the united-atom limit and employing an atomic d orbital function,[2]

$$\phi_{do} = \left(1 + \frac{3}{\gamma r} + \frac{3}{\gamma^2 r^2}\right)\frac{e^{-\gamma r}}{r}\sin\,\theta\cos\,\theta, \tag{5}$$

where $\gamma \propto \sqrt{eBE}$ incorporates the final vibrational state dependence, while r is the distance from the center of mass of the molecule.

The $\beta(E)$ values calculated using the above approach are shown as the dashed curves in Figs. 3 and 4.[71] The calculated $\beta(E)$ trends clearly vary with the vibrational quantum number of the neutral O_2. The ZCC model is the first treatment that attempts to quantitatively describe this behavior for molecular anion detachment.

While overstating the effect of v', the model does reveal why the neutral vibrational state affects β. The appearance of the eBE in ϕ_{do} [Eq. (5)], particularly in the exponential term, is critical. Larger eBE is associated with transitions to higher vibrational levels of O_2. At the same time, larger eBE is associated with a more tightly bound electron and consequently a detachment orbital with a smaller spatial extent. The link between these factors is seen in the potential energy curves for the $O_2(X\ ^3\Sigma_g^-)$ and $O_2^-(X\ ^2\Pi_g)$ states shown in Fig. 5. A Morse potential is used for the anion (with parameters taken from Ref. 27), and the RKR parameters in Ref. 72 produce the neutral curve. The increase in binding energy at greater internuclear separation (R_{OO}) is clearly seen in the divergence of the two potentials, meaning that the spatial extent of the detachment orbital changes throughout the cycle of anion zero-point motion. The main contributions to the vibrational overlap integral occur at different R_{OO} for different vibrational transitions. The integrand is largest where the product of the neutral and anion wave functions is greatest. This condition is met near the outer turning point of the neutral vibration (with the exception of $v'=0$). Since the transition from the anion is vertical (within the Born–Oppenheimer approximation), a detachment via different vibronic transitions preferentially selects different subsets of anion R_{OO}.

The changing spatial extent of the detachment orbital necessarily alters M^e for a given k, and so the E dependence will change with v'. The vibrational dependence of $\beta(E)$ is a direct consequence of Born–Oppenheimer behavior. The reason for the phase changes extracted by application of Eq. (2) in Table I is not transparent in this approach. However, it does offer a rationalization for the behavior of the A parameter in the application of the atomic model of Eq. (2). The A coefficient represents a measure of anion size.[65] The "contradiction" arises from a lack of clarity in the meaning of size in the molecular picture we have outlined, where preferential detachment from larger R_{OO} corresponds to smaller A. Rather than internuclear separation, size here refers to the spatial extent of the detachment orbital.

The above discussion identifies the vibrational level dependence of $\beta(E)$ to be a direct result of variation in the electronic matrix element with R_{OO}. As supporting evidence, a further manifestation of this behavior is found in the variation in transition intensities across the $O_2(X\ ^3\Sigma_g^-) \leftarrow O_2^-(X\ ^2\Pi_g)$ band. In the absence of vibronic coupling, the relative intensities should be reproduced by $F(v',v'')$.[73,74]

Figure 6 compares $F(v',0)/F(2,0)$ [open circles] with the $O_2(X\ ^3\Sigma_g^-) \leftarrow O_2^-(X\ ^2\Pi_g)$ band of our 454.54 nm spectrum. The Franck–Condon factors were calculated using Morse oscillator wave functions[75] employing the spectroscopic constants in Ref. 27 and evaluating the vibrational overlap integral numerically using a 600 point Simpson's method calculation. It is clear that these Franck Condon factors (FCFs) are a poor representation of the spectral intensities, particularly at higher v', showing the influence of vibronic coupling.

It is instructive to compare this finding with the Franck-Condon (FC) treatment of the spectrum given in Ref. 27. The latter work shows that the intensity variation in the $X\ ^3\Sigma_g^- \leftarrow X\ ^2\Pi_g$ band recorded at 364 nm is very well described by the Franck–Condon factors alone. The key difference is the increased photon energy. The vibrational transition intensities can be calculated using the same ZCC approach applied above, integrating Eq. (3) over all angles,

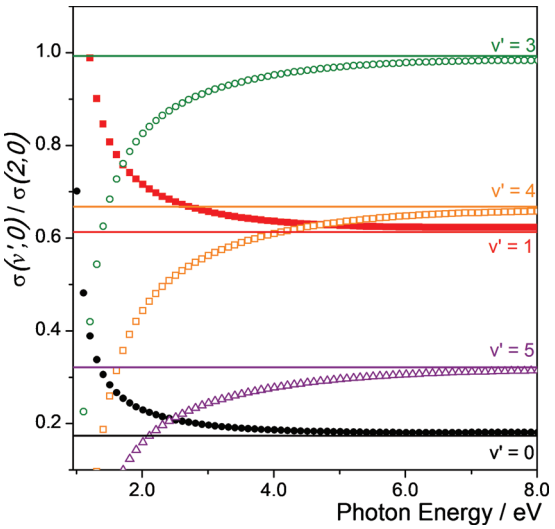

FIG. 7. ZCC total cross sections (symbols) and Franck–Condon factors (solid lines) for $O_2(X\,^3\Sigma_g^-) \leftarrow O_2^-(X\,^2\Pi_g, v''=0)$ transitions relative to $O_2(X\,^3\Sigma_g^-, v'=2) \leftarrow O_2^-(X\,^2\Pi_g, v''=0)$.

$$\sigma(v',v'') = F(v',v'')k\omega \int\int |M^e|^2 d\Omega_m d\Omega. \tag{6}$$

The variation in relative transition intensities [effectively $\sigma(v',0)/\sigma(2,0)$] is shown in Fig. 7. At photon energies close to threshold, there is considerable deviation from the Franck–Condon prediction (the horizontal lines). However, as the photon energy increases the values converge, a result of the dependence of the cross section (and M^e) on k. The trends in E and the vibrational dependence of the overall cross sections for O_2^- detachment will be dealt with thoroughly in a forthcoming publication.[76]

Agreement between the ZCC calculation of $\beta(E)$ and experiment is not particularly good. A comparison of the united-atom orbital and a more realistic linear combination of atomic p orbitals as the detachment orbital reveals that the atomic d orbital approximation makes little difference to the result of the calculation.[2] However, more significant errors are introduced in the nature of the ZCC model itself. As E increases, the de Broglie wavelength becomes comparable with the dimensions of the core region, in which case zero core contribution will no longer be a good approximation.[57] Additionally, the employment of the one-electron approximation and assumption of no interaction between the detachment and core electrons implicitly neglects electron correlation effects that are known to be strongly influential in anionic species.[77] Nevertheless, as a means of illustrating the effect of the changing spatial extent of ϕ_{do} on the vibrational dependence of $\beta(E)$, the model is enlightening. It should also be pointed out that more sophisticated models that include many-body effects have so far neglected the influence of product vibration on the photoelectron angular distributions. Furthermore, recent multi-configuration single excited configuration interaction (MCSCI) (Ref. 55) and equation of motion-coupled cluster (EOM-CC) (Ref. 56) calculations consistently underestimate the magnitude of the β parameter from the $O_2(X\,^3\Sigma_g^-, v'=0) \leftarrow O_2^-(X\,^2\Pi_g, v''=0)$ transition. The results presented here extend the previous systematic experimental study of the vibrational dependence of photodetachment angular distributions from O_2^-.[1] The clear implication of these results, particularly in the context of existing models, is that there is a need for additional studies of this type, which will form vital benchmark tests of theoretical treatments of negative ions.

V. CONCLUSION

To summarize, we have experimentally demonstrated that the variation of β with E for molecular anion detachment depends on the level of neutral molecule vibrational excitation. While the quantitative agreement with the experimental data is not perfect, the simple one-electron ZCC model allows us to interpret this behavior in terms of the changes in the electronic transition matrix element. There is significant coupling of the electronic and nuclear motion in the ground state of the anion, and the experimentally determined $\beta(E)$ values are significantly different to those predicted by the latest quantum chemical treatments.

ACKNOWLEDGMENTS

The authors gratefully acknowledge support by the National Science Foundation (Grant No. CHE-0748738) and ANU ARC Discovery Projects under Grant Nos. DP0666267 and DP0880850. We also thank Professor B. J. Orr for discussions regarding treatment of diatomic anion angular distributions.

[1] R. Mabbs, F. Mbaiwa, J. Wei, M. Van Duzor, S. T. Gibson, S. J. Cavanagh, and B. R. Lewis, Phys. Rev. A **82**, 011401(R) (2010).
[2] R. M. Stehman and S. B. Woo, Phys. Rev. A **23**, 2866 (1981).
[3] J. Simons, J. Phys. Chem. A **112**, 6401 (2008).
[4] E. P. Wigner, Phys. Rev. **73**, 1002 (1948).
[5] H. A. Bethe, in *Handbuch der Physik*, edited by H. Geiger and W. Scheel (Springer, Berlin, 1933), Vol. 24, p. 483.
[6] J. Cooper and R. N. Zare, in *Atomic Collision Processes*, edited by S. Geltman, K. T. Mahanthappa, and W. E. Brittin (Gordon and Breach, New York, 1968), Vol. 11-C, p. 317.
[7] J. M. Sichel, Mol. Phys. **18**, 95 (1970).
[8] R. Mabbs, E. R. Grumbling, K. Pichugin, and A. Sanov, Chem. Soc. Rev. **38**, 2169 (2009).
[9] B. Ritchie, Phys. Rev. A **13**, 1411 (1976).
[10] B. Ritchie, Phys. Rev. A **14**, 359 (1976).
[11] N. Chandra, J. Phys. B **20**, 3405 (1987).
[12] J. G. Underwood and K. L. Reid, J. Chem. Phys. **113**, 1067 (2000).
[13] K. L. Reid and J. G. Underwood, J. Chem. Phys. **112**, 3643 (2000).
[14] O. Geßner, A. M. D. Lee, J. P. Shaffer, H. Reisler, S. V. Levchenko, A. I. Krylov, J. G. Underwood, H. Shi, A. L. L. East, D. M. Wardlaw, E. H. Chrysostom, C. C. Hayden, and A. Stolow, Science **311**, 219 (2006).
[15] A. Stolow and J. G. Underwood, Adv. Chem. Phys. **139**, 497 (2008).
[16] K. J. Reed, A. H. Zimmerman, H. C. Andersen, and J. I. Brauman, J. Chem. Phys. **64**, 1368 (1976).
[17] R. Mabbs, E. Surber, and A. Sanov, Chem. Phys. Lett. **381**, 479 (2003).
[18] A. Sanov and R. Mabbs, Int. Rev. Phys. Chem. **27**, 53 (2008).
[19] P. C. Cosby, R. A. Bennett, J. R. Peterson, and J. T. Moseley, J. Chem. Phys. **63**, 1612 (1975).
[20] P. C. Cosby, J. H. Ling, J. R. Peterson, and J. T. Moseley, J. Chem. Phys. **65**, 5267 (1976).
[21] D. S. Burch, S. J. Smith, and L. M. Branscomb, Phys. Rev. **112**, 171 (1958).
[22] D. S. Burch, S. J. Smith, and L. M. Branscomb, Phys. Rev. **114**, 1652 (1959).
[23] R. A. Beyer and J. A. Vanderhoff, J. Chem. Phys. **65**, 2313 (1976).
[24] J. A. Burt, Can. J. Phys. **50**, 2410 (1972).
[25] R. V. Hodges, L. C. Lee, and J. T. Moseley, J. Chem. Phys. **72**, 2998 (1980).

[26] L. C. Lee and G. P. Smith, J. Chem. Phys. **70**, 1727 (1979).
[27] K. M. Ervin, I. Anusiewicz, P. Skurski, J. Simons, and W. C. Lineberger, J. Phys. Chem. A **107**, 8521 (2003).
[28] R. J. Celotta, R. A. Bennett, J. L. Hall, M. W. Siegel, and J. Levine, Phys. Rev. A **6**, 631 (1972).
[29] R. R. Corderman, P. C. Engelking, and W. C. Lineberger, Appl. Phys. Lett. **36**, 533 (1980).
[30] M. J. Travers, D. C. Cowles, and G. B. Ellison, Chem. Phys. Lett. **164**, 449 (1989).
[31] K. M. Ervin and W. C. Lineberger, in *Advances in Gas Phase Ion Chemistry*, edited by L. M. Babcock (JAI, Greenwich, 1992), Vol. 1, p. 121.
[32] C. G. Bailey, D. J. Lavrich, D. Serxner, and M. A. Johnson, J. Chem. Phys. **105**, 1807 (1996).
[33] K. A. Hanold, C. R. Sherwood, M. C. Garner, and R. E. Continetti, Rev. Sci. Instrum. **66**, 5507 (1995).
[34] U. Boesl, C. Bassmann, and R. Kassmeier, Int. J. Mass. Spectrom. **206**, 231 (2001).
[35] F. A. Akin, L. K. Schirra, and A. Sanov, J. Phys. Chem. A **110**, 8031 (2006).
[36] A. K. Luong, T. G. Clements, M. Sowa Resat, and R. E. Continetti, J. Chem. Phys. **114**, 3449 (2001).
[37] K. Le Barbu, J. Scheidt, R. Weinkauf, E. W. Schlag, J. M. Nilles, S. J. Xu, O. C. Thomas, and K. H. Bowen, Jr., J. Chem. Phys. **116**, 9663 (2002).
[38] C. Kang, J. L. Troyer, E. M. Robertson, D. W. Rothgeb, E. Hossain, R. B. Wyrwas, C. S. Parmenter, and C. C. Jarrold, J. Chem. Phys. **128**, 104309 (2008).
[39] L. Velarde, T. Habteyes, E. R. Grumbling, K. Pichugin, and A. Sanov, J. Chem. Phys. **127**, 084302 (2007).
[40] T. A. Carlson, Chem. Phys. Lett. **9**, 23 (1971).
[41] T. A. Carlson and A. E. Jonas, J. Chem. Phys. **55**, 4913 (1971).
[42] J. L. Dehmer, D. Dill, and S. Wallace, Phys. Rev. Lett. **43**, 1005 (1979).
[43] J. Cooper and R. N. Zare, J. Chem. Phys. **48**, 942 (1968).
[44] B. Ritchie, J. Chem. Phys. **60**, 898 (1974).
[45] A. D. Buckingham, B. J. Orr, and J. M. Sichel, Philos. Trans. R. Soc. London **268**, 147 (1970).
[46] U. Fano and D. Dill, Phys. Rev. A **6**, 185 (1972).
[47] D. Dill, Phys. Rev. A **6**, 160 (1972).
[48] Y. Itikawa, Chem. Phys. **28**, 461 (1978).
[49] Y. Itikawa, Chem. Phys. **30**, 109 (1978).
[50] N. Chandra, Chem. Phys. **108**, 301 (1986).
[51] M. Raoult, C. Jungen, and D. Dill, J. Chem. Phys. **77**, 599 (1980).
[52] J. C. Tully, R. S. Berry, and B. J. Dalton, Phys. Rev. **176**, 95 (1968).
[53] W. Thiel, Chem. Phys. **77**, 103 (1983).
[54] G. Raşeev and N. A. Cherepkov, Phys. Rev. A **42**, 3948 (1990).
[55] P. Lin and R. R. Lucchese, J. Chem. Phys. **114**, 9350 (2001).
[56] C. M. Oana and A. I. Krylov, J. Chem. Phys. **131**, 124114 (2009).
[57] R. M. Stehman and S. B. Woo, Phys. Rev. A **20**, 281 (1979).
[58] S. J. Cavanagh, S. T. Gibson, M. N. Gale, C. J. Dedman, E. H. Roberts, and B. R. Lewis, Phys. Rev. A **76**, 052708 (2007).
[59] E. H. Roberts, S. J. Cavanagh, S. T. Gibson, B. R. Lewis, C. J. Dedman, and G. J. Picker, J. Electron Spectrosc. Relat. Phenom. **144–147**, 251 (2005).
[60] C. J. Dedman, E. H. Roberts, S. T. Gibson, and B. R. Lewis, Rev. Sci. Instrum. **72**, 2915 (2001).
[61] A. T. J. B. Eppink and D. H. Parker, Rev. Sci. Instrum. **68**, 3477 (1997).
[62] E. W. Hansen and P.-L. Law, J. Opt. Soc. Am. A **2**, 510 (1985).
[63] F. Breyer, P. Frey, and H. Hotop, Z. Phys. A **286**, 133 (1978).
[64] J. L. Hall and M. W. Siegel, J. Chem. Phys. **48**, 943 (1968).
[65] D. Hanstorp, C. Bengtsson, and D. J. Larson, Phys. Rev. A **40**, 670 (1989).
[66] R. Mabbs, E. Surber, and A. Sanov, J. Chem. Phys. **122**, 054308 (2005).
[67] F. Mbaiwa, M. Van Duzor, J. Wei, and R. Mabbs, J. Phys. Chem. A **114**, 1539 (2010).
[68] F. Mbaiwa, J. Wei, M. Van Duzor, and R. Mabbs, J. Chem. Phys. **132**, 134304 (2010).
[69] J. Cooper and R. N. Zare, J. Chem. Phys. **49**, 4252 (1968).
[70] R. M. Stehman, Ph.D. dissertation, University of Delaware, 1980.
[71] In performing these calculations, we discovered a typographical error in Eq. (31) of Ref. 2, which should read as $I_1 = \int\int \sin\theta \cos\theta \cos(kr \cos\beta \cos\theta) J_1(kr \sin\beta \sin\theta) f(r,\theta) r^3 dr d\theta$.
[72] P. H. Krupenie, J. Phys. Chem. Ref. Data **1**, 423 (1972).
[73] P. A. Fraser, Can. J. Phys. **32**, 515 (1954).
[74] R. W. Nicholls, J. Quant. Spectrosc. Radiat. Transf. **2**, 433 (1962).
[75] M. Halmann and I. Laulicht, J. Chem. Phys. **43**, 438 (1965).
[76] S. T. Gibson, S. J. Cavanagh, B. R. Lewis, J. R. Gascooke, R. Mabbs, B. J. Orr, H. Lefebvre-Brion, and R. R. Lucchese (unpublished).
[77] V. K. Ivanov, Radiat. Phys. Chem. **70**, 345 (2004).